Int. J. Electrochem. Sci., 17 **(2022)** Article Number: 220967, doi: 10.20964/2022.09.62

International Journal of
ELECTROCHEMICAL
SCIENCE
www.electrochemsci.org

Preparation of RuO_2/CNTs by Atomic Layer Deposition and its application as binder free Cathode for polymer based Li-O_2 battery

Norah Algethami[1,†], *Hend I. Alkhammash*[2], *Fozia Sultana*[3,†,*], *Muhammad Mushtaq*[4], *Abid Zaman*[5,*], *Asad Ali*[6], *Khaled Althubeiti*[7], *Qing Yang*[8].

[1] Department of Physics, Faculty of Science, Taif University, P.O. Box 11099, Taif 21944, Saudi Arabia.
[2] Department of Electrical Engineering, College of Engineering, Taif University, Taif 21944, Saudi Arabia.
[3] Department of Chemistry, University of Science and Technology China, Hefei 230026, China
[4] Faculty of Materials Science, Beijing University of Technology, Beijing 100124, China.
[5] Department of Physics, Riphah International University, Islamabad 44000, Pakistan.
[6] Department of Physics, Government Post Graduate College, Nowshera 24100, Pakistan.
[7] Department of Chemistry, College of Science, Taif University, P.O. Box 11099, Taif 21944, Saudi Arabia.
[8] Hefei National Laboratory of Physical Sciences at the Microscale (HFNL), Department of Chemistry, Laboratory of Nanomaterial's for Energy Conversion (LNEC), University of Science and Technology China, Hefei 230026, Anhui, P. R. China.
[*]E-mail: zaman.abid87@gmail.com (A.Z) & fsultana@mail.ustc.edu.cn (F.S)
[†]These authors contributed equally to this work.

Received: 4 June 2022 / *Accepted:* 17 July 2022 / *Published:* 7 August 2022

Polymer-based (Li-O_2) battery have paid much more devotions owing to their safety as compared to conventional liquid electrolyte batteries. However, the carbon-based cathode with polymer binder shows serious degradations in the electrochemical performance of Li-O_2 batteries due to parasitic decomposition reactions during operation of battery. Therefore, it is highly indispensable to develop a cathode that builds vigorous and outstanding performance in Li-O_2 batteries. Herein, a binder-free cathode of carbon nanotubes (CNTs) have been fabricated by surface modification using RuO_2 catalyst through ALD approach. A solid catalyst of RuO_2 has been deposited on CNTs defects sites which not only stopes the decomposition of carbon but also endorse the reversible accumulation and breakdown of Li_2O_2 on cathode surface. The CNT/RuO_2 cathode with the distinctive structure illustrate excellent performance by showing a small potential gap of 0.6V at mid-point and better cycle stability without large capacity decay over 50 cycles. This study demonstrates that the surface engineering of carbon cathode could be a favorable approach to develop Li-O_2 batteries.

Keywords: Polymer based Li-O_2 battery; Binder-free cathode; RuO_2 catalyst; low potential gap.

1. INTRODUCTION

Lithium-oxygen batteries are currently attracting a lot of interest due to their higher energy density than Li-ion batteries. Although, the oxygen reduction reaction (ORR) and oxygen evolution reaction (OER) result in the formation and reversible breakdown of the discharge product Li_2O_2 into O_2 during Li-O_2 battery operation [1-5]. Since Li-O_2 battery introduction in 1996, the system has faced various scientific and technical challenges that must be addressed. some of these challenges are the evaporation of organic electrolytes during discharge and charge process and the decomposition of discharge product from the cathode surface, that causes instability in Li-O_2 batteries [6-9]. Moreover, the excessive deposition of discharge product Li_2O_2 on cathode surface blocks the continuous diffusion of oxygen gas, which eventually effects the battery performance including specific capacity, charge potential and cycling stability [10-13]. Additionally, the continuous deposition of lithium carbonate (Li_2CO_3) and lithium carboxylates caused by the instability of Li_2O_2 with electrolyte and polymer binder trigger cathode passivation and eventually batteries death [14-16]. Although great progress has been made, the improvements do not yet outweigh the foregoing challenges, which prevent Li-O_2 batteries from becoming commercially viable. Another issue that needs to be addressed is the apparent increase in defect sites that occurs during repeated discharge and charge. It has been reported in the previous studies, that the carbon cathodes can be stabilized by passivating the surface defects through chemically stable materials [17-21]. As a result, it is critical to design and build a highly efficient cathode with a specific architecture that can significantly influence both ORR and OER in order to improve the performance of Li-oxygen batteries. The optimum cathode for Li-O_2 batteries should have high electronic conductivity, great porosity to accommodate abundant discharge product, smooth oxygen diffusion, and sufficient catalytic activity for the breakdown of discharge products [22-24]. Several efforts have been made to pursuit effective catalysts with sufficient catalytic activity including noble metals [25,26], metal oxides [27,28] metal nitrides [29,30] and carbides [31,32]. Among them, RuO_2 has been observed as one of the widely used catalysts for endorsing ORR and OER in Li-O_2 batteries [33,34]. Moreover, the surface engineering approaches of carbon cathode reported previously have demonstrated significant improvement in the cycle stability of Li-O_2 batteries [35-38]. Thus, implementing efficient catalysts in carbon-based cathodes that can decompose both Li_2O_2 and Li_2CO_3 at lower charge potentials should be a promising strategy for improving Li-O_2 battery electrochemical activity. However, the procedure is complicated and time-consuming since it involves two phases: metal oxides coating followed by noble metals. A "binder-free" carbon nanotube (CNT) cathode with RuO_2 nanoparticles coating has been claimed to improve rechargeability under low charge potential and shield the carbon surface during Li-O_2 battery operation [39-41]. Herein, the RuO_2 has been developed by Atomic Layer Deposition method as an electrocatalyst for Li-O_2 batteries. According to scanning electron microscopy SEM and electrochemical performance, the incorporation of RuO_2 catalyst in cathode formation not only protect the carbon nanotubes surface from decomposition but synergistically reduce the charge potential during charging of Li-O_2 battery. The overpotential is reduced from 1.40V to 0.6V, which is the obvious indication of RuO_2 catalysts for removal of discharge product at lower charge potential. Moreover, the distinctive porous structure of composite cathode leads to provide a continuous diffusion of oxygen, abundant space to accommodate large amount of discharge products and provide more active sites. The

Li-O_2 batteries based on RuO_2/CNT composite cathode has shown clearly reduced overpotential and improved cycling stability.

2. EXPERIMENTAL SECTION

2.1. Materials

The modified silyl-terminated polyether (MSTP) monomer, Tetra ethylene glycol dimethyl ether (TEGDME, 99.9%), lithium bis (trifluoromethane sulfonamide) (LiTFSI, 99.95%), Tin catalyst (Tin), N-methyl-2-pyrrolidinone (NMP) Carbon nanotubes (CNTs) and Ruthenium dioxide (RuO_2), Nitric acid (HNO_3) and deionized water (DI) were bought from Aladdin, and placed in the glove box.

2.2. Preparation of polymer electrolytes

The polymer electrolyte has been prepared by simple solution casting method in which 1.75g LiTFSI salt was dissolved in 2.5 mL TEGDME solution. Afterward, 0.75g methyl silyl terminated polyether (MSTP) was mixed with the as-prepared solution and stirred for 40 minutes to obtain a homogenous solution. In order to speed up the polymerization rate, 20 µL tin catalyst was added to synthesize precursor solution and stirred it for further 10 minutes. The precursor solution was poured into the Whatman filter paper which give mechanical strength to polymer film. The pores of the Whatman paper were filled with the polymer precursor. The solution was then shifted to vacuum oven for drying at 60^{o}C for 3 hours. The polymer electrolyte was transferred to another oven for further drying at 80^{o}C for more 2 hours. After all these steps, the MSTP based polymer electrolyte was obtained used for characterizations and electrochemical tests in Li-O_2 battery.

2.3. Fabrication of CNT/RuO_2 cathode

The composite cathode of CNT/RuO_2 was synthesized by atomic layer deposition method. The carbon nanotubes were washed by ultrasonication method with 40% dilute solution of HNO_3. The ultrasonicated CNTs were centrifuged and washed three times with deionized water to remove remedies. The collected CNTs were dried at 80^{o}C for 12 hours. After that, the CNTs solution was prepared in NMP solvent, and binder free cathode was prepared by simple filtration method. The CNTs coated carbon papers were then shifted to deposit RuO_2 for 200, 400 and 800 ALD cycles. The composite cathode of CNTs coated with 400 ALD cycles were used as an active material in testing the electrochemical performance of the Li-O_2 batteries. The Carbon paper (Toray Company) was utilized as the current collector with mass loading of CNT/RuO_2 from 3.0 ~ 5.0 mg cm^{-2}.

2.4 Li-O_2 Cell Assembly and Characterizations.

The Li-O_2 cells were assembled an Ar filled glove box having water and oxygen concentration less than 0.1ppm. A polymer electrolyte film of MSTP is employed between cathode and anode. The cell was oxygenated for 20 minutes through the gas inlet and outlet in the home made glass bottle to provide pure oxygen environment. The bottle was carefully sealed to enclose the oxygen for battery operation. For conducting discharge-charge tests, Land battery system was used. Moreover, the fluctuation in specific capacity can be calculated on basis of CNTs weight on carbon paper.
The ionic conductivity of polymer electrolyte film was deliberated by Electrochemical Impedance Spectroscopy (EIS) via Versa STAT 3 system at room temperatures. To record the spectra in the frequency, range from 0.1 to 105 Hz using 10 mV AC amplitude, the polymer film was sandwiched between two stainless steel plates. The bulk resistance (R_b) of the polymer film was calculated by using the impedance spectrum. Using the equation ($\sigma = d/R_bS$), the ionic conductivity was calculated, where R_b denotes the bulk resistance, d is the thickness of the film and S is area of the polymer film, respectively. Ex-Situ SEM was used to study the morphology of discharge product formed on the cathode surface after disassembling of the fully discharge Li-O_2 battery in an Ar filled glove box. For X-ray analysis, Cu Kα radiation (λ=1.5406) was used for X-ray diffraction with a Bruker D8 Focus Power X-ray diffract meter. To stop the air reaction with discharge product, the samples were put onto a glass substrate and afterward wrapped with a Kapton polyimide sheet. Ex-situ SEM, XRD, Raman and XPS have been used to investigate each composite cathodes of pristine, discharged, and recharged phases, respectively. For SEM, XRD Raman and XPS characterization, the discharged and recharged composite cathodes were transferred for testing without exposing to air for a long period of time.

3. RESULTS AND DISCUSSION

The polymer electrolyte film was blended by simple solution casting approach, which has been explained in the previous reports [42-44]. An appropriate ionic conductivity is one of the major aspect for the enhancement of electrochemical performance in polymer based Li-O_2 batteries. The ions transformation ability of as-prepared polymer film is determined from the intercept on the real axis at room temperature using bulk resistance (R_b) as shown in Fig.1a. The estimated ionic conductivity for polymer electrolyte is 1.3 10^{-4} S cm^{-1}, which is comparable to liquid electrolyte and beneficial for boosting the electrochemical performance of Li-O_2 batteries. Therefore, it demonstrates, that the as-prepared polymer film has satisfactory ionic conductivity to be utilized in Li-O_2 batteries. The ionic conductivity of polymer film was calculated by using the formula $\sigma = d/ R_b S$ where d is the thickness of polymer film, S is the surface area (diameter Φ = 16 mm) and R_b is the bulk resistance [45]. Another important property of the polymer electrolyte is its thermal durability. The thermo-gravimetric TG and differential scanning calorimetry (DSC) curves in Fig.1b demonstrate that the polymer electrolyte with whatman paper framework can retain its stability below 150 ℃, which is critical for improving safety as compared to a liquid electrolyte at elevated temperatures. The polymer starts electrolyte begins melting at 200°C, as evidenced by the prominent DSC peak. Moreover, the polymer film with application of whatman paper filter provides high mechanical strength and smooth surface as shown in Fig.1c. The inset of Fig.1c shows the flexibility of polymer film, which is suitable for application in foldable devices

and easy to handle in assembling Li-O_2 batteries. Furthermore, the smooth surface and high flexibility of polymer electrolyte is beneficial for enhancing the electrochemical performance and better interfacial contacts with electrodes in Li-O_2 batteries.

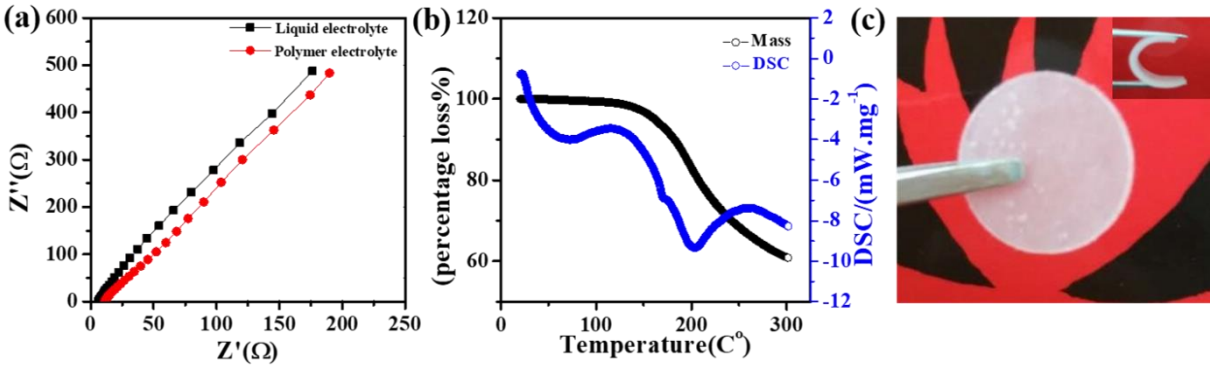

Figure 1. (a) Electrochemical impedance spectroscopy of Stainless steel/Polymer electrolyte/ Stainless steel at room temperature **(b)** Thermo-gravimetric (TG) and Differential Scanning Calorimetry (DSC) curves of Polymer electrolyte film **(c)** Photograph of polymer electrolyte and the in-sit shows the flexibility of polymer film.

The surface morphology of both CNT and composite cathode of CNT/RuO_2 was investigated using SEM. According to Fig.2a, the CNT cathode has a porous framework with a large surface area, which is required for a higher specific capacity in Li-O_2 batteries. The carbon cathode has enough gas diffusion paths and has adequate active sites for the accommodation of discharge products. After fabricating the composite cathode by atomic layer deposition method, RuO_2 catalyst is deposited on the active sites of CNTs uniformly as shown in Fig. 2b. The elemental distributions of C, O and Ru in CNT/RuO_2 composite cathode are explored by Energy Dispersive X-ray spectroscopy (EDS) as demonstrated in Fig. 2(c & d). The EDS results depict that the RuO_2 nanoparticles have uniformly distributed on CNTs surface. Thus, it is concluded that RuO_2 nanoparticles deposited on the surface of CNTs not only circumvent it from passivation but also contribute widely for the breakdown of Li_2O_2 during charge process.

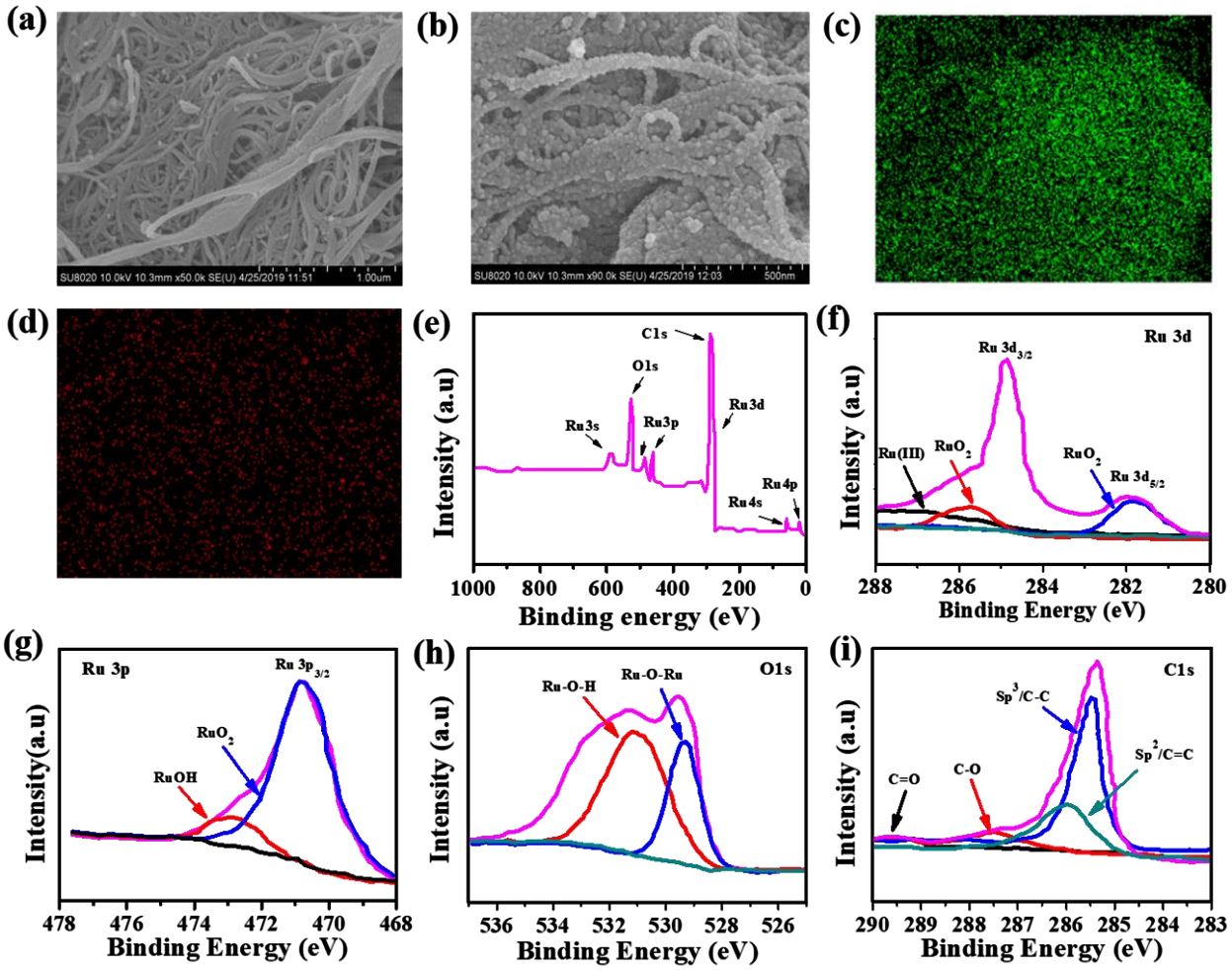

Figure 2. The SEM images of the (a) pristine CNTs and (b) composite cathode with deposition of RuO_2 catalyst (c) show EDX mapping for carbon element (d) Ruthenium element. (e) Shows the X-ray photoelectron spectroscopic analysis of CNT/RuO_2 (f) spin-orbit of Ru (g) Ru 3p (h) O 1s and (i) C 1s spectra of CNT in CNT/RuO_2 cathode.

Furthermore, the CNT framework can provide abundant pathways for smooth transport of electrons. The porous cathode of CNT/RuO_2 in polymer-based Li-O_2 batteries, as shown in Fig. 2b, has sufficient reaction sites, an interconnected framework of CNTs for electron transport, and smooth gas flow. Considering the advantages listed above, the electrochemical processes on the CNT/RuO_2 cathode surface are far more easy. Furthermore, the porous nature of the composite cathode can accommodate a considerable amount of discharge products, allowing for a high specific capacity.

The elemental composition and valence state of the composite cathode were determined using X-ray photoelectron spectroscopy (XPS) analysis. In Fig. 2e, the typical XPS spectrum for RuO_2/CNTs shows numerous peaks that confirm the presence of C, O, and Ru components. Ru 3d has 3/2 and 5/2 spin-orbit regions of 284.5 and 281.3 eV, respectively, as shown in Fig. 2f, whereas Ru 3p has a significant peak at 463.5 eV, as seen in Fig. g. The Ru $3d_{5/2}$ binding energy is 281.3 eV, which overlaps somewhat with the C 1s peak and corresponds to the Ru^{4+} oxidation state in metallic Ru (280 eV). Furthermore, two new segments have arisen at 286.0 and 284.8 eV, which are typically assigned to Ru

(III) and RuO_2 respectively. Furthermore, the O 1s XPS spectrum (Fig .2h) reveals a peak at 529.8 eV, which corresponds to Ru-O-Ru bond. The C 1s spectra of CNTs in CNTs/ RuO_2 is shown in Fig. 2i, with two prominent peaks at 284.9 eV and 285.9 eV corresponding to C=C graphite carbon, C–C, bonds in produced materials. The presence of the C–C peak suggests the presence of defects in the structure of CNTs.

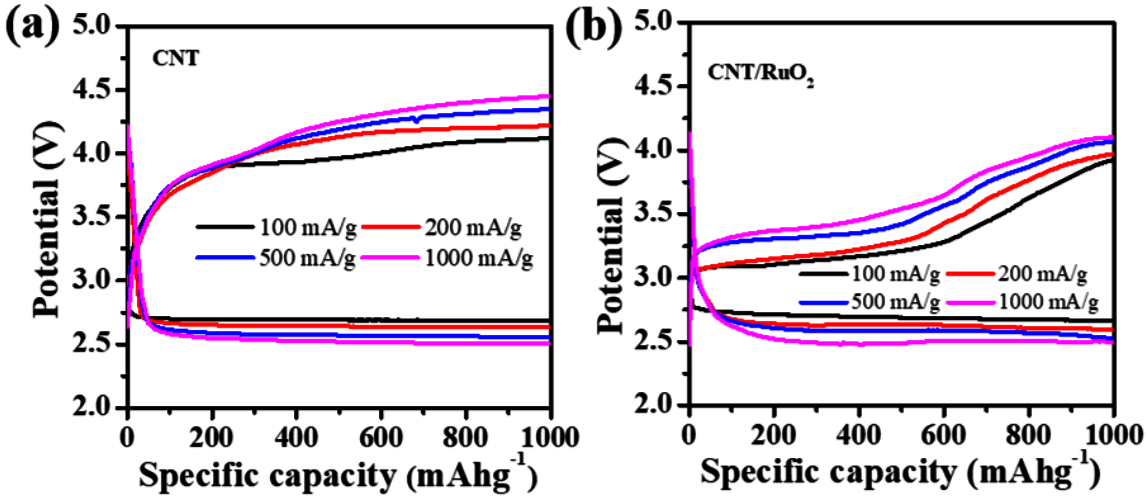

Figure 3. (a) Discharge-charge curves for polymer electrolyte based Li-O_2 batteries with CNT cathode and (b) CNT/RuO_2 based cathode at different current rate ranging from 100 to 1000 mAg^{-1} at limited capacity of 1000 $mAhg^{-1}$.

The cathode has been designed and developed to promote the kinetics for OER reaction during the charge process in Li-O_2 batteries using a carbon-based cathode with/without RuO_2 catalyst. During the rate performance of the polymer-based Li-O_2 battery with CNT cathode shown in Fig. 3a, a substantial charge potential of nearly 4.45V was achieved. Furthermore, the rate performance seems unsatisfactory at elevated current density (1000 mA g^{-1}) because of unsatisfactory ionic conductivity of polymer electrolyte, low electronic conductivity of Li_2O_2 and poor kinetics for decomposition of Li_2O_2 during charge process. In contrast, a CNT/RuO_2 composite cathode has been designed to test the improvement in OER activity and lowering the charge potential. A significant reduction in the potential from 4.45 V to 3.87V has been achieved in the Li-O_2 battery based on the composite cathode of CNT/RuO_2. The outstanding rate performance with low charge potential at high current density has confirmed the contribution of RuO_2 for OER reaction during charge process of Li-O_2 battery. Therefore, the pure CNT cathode was substituted by composite cathode with highly efficient catalyst to enhance the rate capability.

As described above, the CNT/RuO_2 cathode illustrate remarkable catalytic performance for the OER reaction, which can dramatically reduce the charge potential. As a result, the addition of RuO_2 in the cathode fabrication greatly increased the rate performance with synergistic catalytic activity with remarkable reduction in the charge potential at high current density of 1000 mAg^{-1} as shown in Fig. 3b.

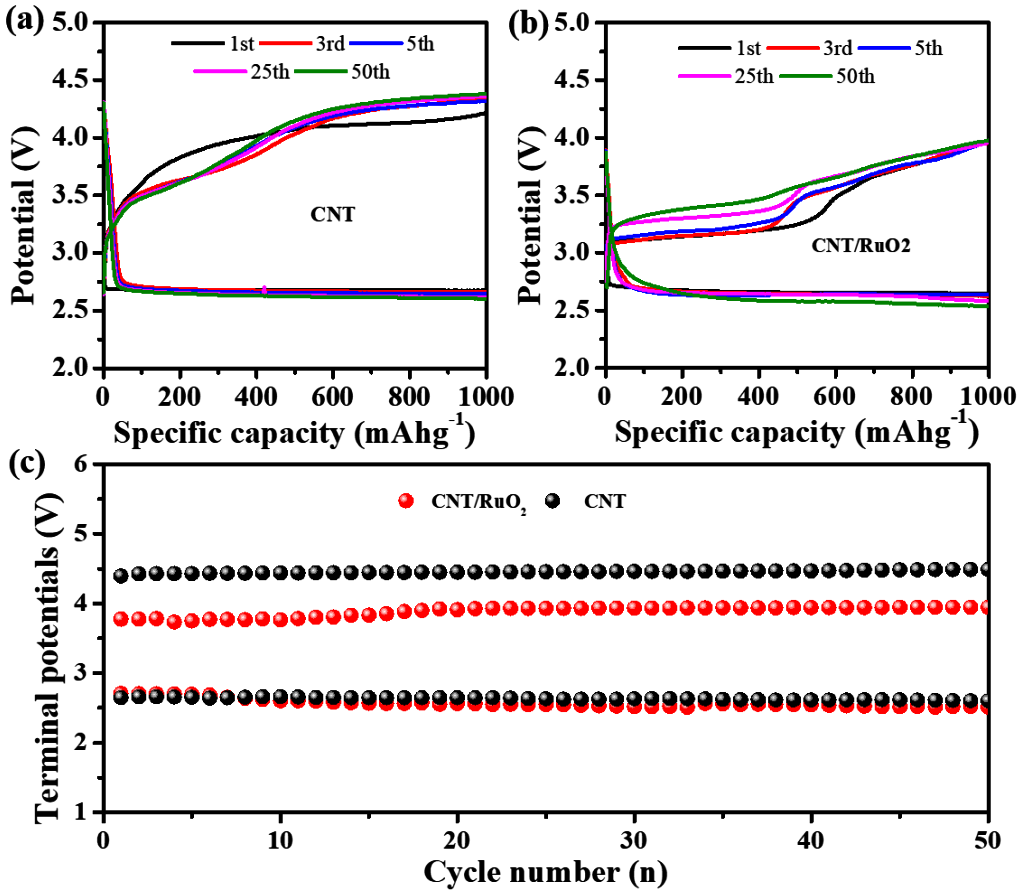

Figure 4. Comparisons of galvanostatic discharge-charge profiles of cycling stability for polymer based Li-Oxygen batteries with **(a)** Pure CNT cathode **(b)** CNT/RuO_2 cathode at current density of 200 $mAhg^{-1}$ with cut off capacity of 1000 $mAhg^{-1}$ **(c)** Comparison of discharge and charge terminal potential of CNT and CNT/RuO_2 based cathode at the same current density.

Furthermore, the galvanostatic discharging and charging profile for cycling stability of Li-O_2 batteries were investigated at current density of 200 mAg^{-1} with curtailing capacity of 1000 $mAhg^{-1}$. The charge potential for the Li-O_2 battery with pure CNT cathode is higher than 4.45V after 50 cycles, as shown in Fig. 4a. It's worth mentioning that polymer-based Li-O_2 without RuO_2 catalyst has poor cycling stability, which could be attributed to the inadequate breakdown of discharge product Li_2O_2 and by products generated during the discharge and charge process, particularly at high overpotential. On the other hand, the incorporation of RuO_2 in CNTs cathode can immensely reduce charge overpotential to the terminal value lower than 3.95 V as shown in Fig. 4b. The reduction of over potential from 1.40V to 0.6V for the CNT/RuO_2 cathode and extended cycling stability for 50 cycles is attributed to the fast kinetics of RuO_2 for OER during charge process. In addition, Fig. 4c compares the charge and discharge terminal potential of polymer-based Li-O_2 batteries with and without RuO_2 catalyst. An obvious decrease in the overpotential is observed for cathode of CNT/RuO_2 based Li-O_2 battery. The reduction in overpotential illustrates the critical role of RuO_2 catalysts in facilitating reversible decomposition of discharge product. The substantial improvement in electrochemical performance is due to the synergistic

effect of CNTs/RuO_2 catalyst on the effective disintegration of Li_2O_2 at the interfacial contact between air cathode and polymer electrolyte. This reduces overpotential and improves cycle stability.

Based on the findings, it is concluded that combining CNT and RuO_2 would significantly improve OER activity in polymer-based Li-O_2 batteries. As a result, we distinguish the cathode structure with adequate catalyst deposition using appropriate method as key characteristics impacting cycling stability in polymer Li-O_2 batteries. In addition, some previous reports using RuO_2 catalyst coated on carbon surface through various approaches have been compared to our work in the table 1. It is concluded, that Li-O_2 battery using CNT/RuO_2 via Atomic Layer Deposition method have shown better consistency between 1st and last charge potentials. The stable charge potential for 50 cycles has been indorsed to the effective contribution of RuO_2 catalyst for improving OER reaction during charging of Li-O_2 battery.

Table 1. Comparison of terminal charge stability using RuO_2 catalyst in cathode

Catalyst	Methods of preparation	Terminal charge potential of 1st and last cycle	Ref
RuO_2/CNT	Atomic Layer Deposition	3.94-3.95V	This work
TiO_2@RuO_2/KB	Sol-gel method	3.9-4.5V	49
RuO_2/NiNCs	Hydrothermal method	3.6-4.5V	50
RuO_2@MnO_2/CNT	Vacuum filtration method	4.2-4.5V	51
RuO_2@LSCF-NFs	Co-precipitation method	4.2-4.3V	52
RuO_2@GNRs	Co-precipitation method	3.5-4.5V	53
RuO_2+TTF/CNT	Hydrothermal method	3.6-4.05V	54
RuO_2@MnO_2-TIT	Electrospinning	4.50-4.55V	55
α-MnO_2@RuO_2/XC-72	Hydrothermal method	4.1-4.0V	56
RuO_2@MnO_2/Ni/G	Solution impregnation method	3.5-4.5V	57

Furthermore, SEM, XRD, and Raman characterization were performed for discharged and recharged cathodes to explore the structure of discharge yields and the reversibility of creating and breaking down Li_2O_2 under pure oxygen atmosphere. A thin film-like morphology of discharge product

Li_2O_2 appears on the CNTs surface [45,46] has been observed in the SEM images collected after discharging (Fig. 5a), while after successive recharge of cathode, most of the discharge product Li_2O_2 are removed (Fig. 5b) [47]. These findings clearly reveal the contribution of RuO_2 for the reversible decay of discharge product Li_2O_2.

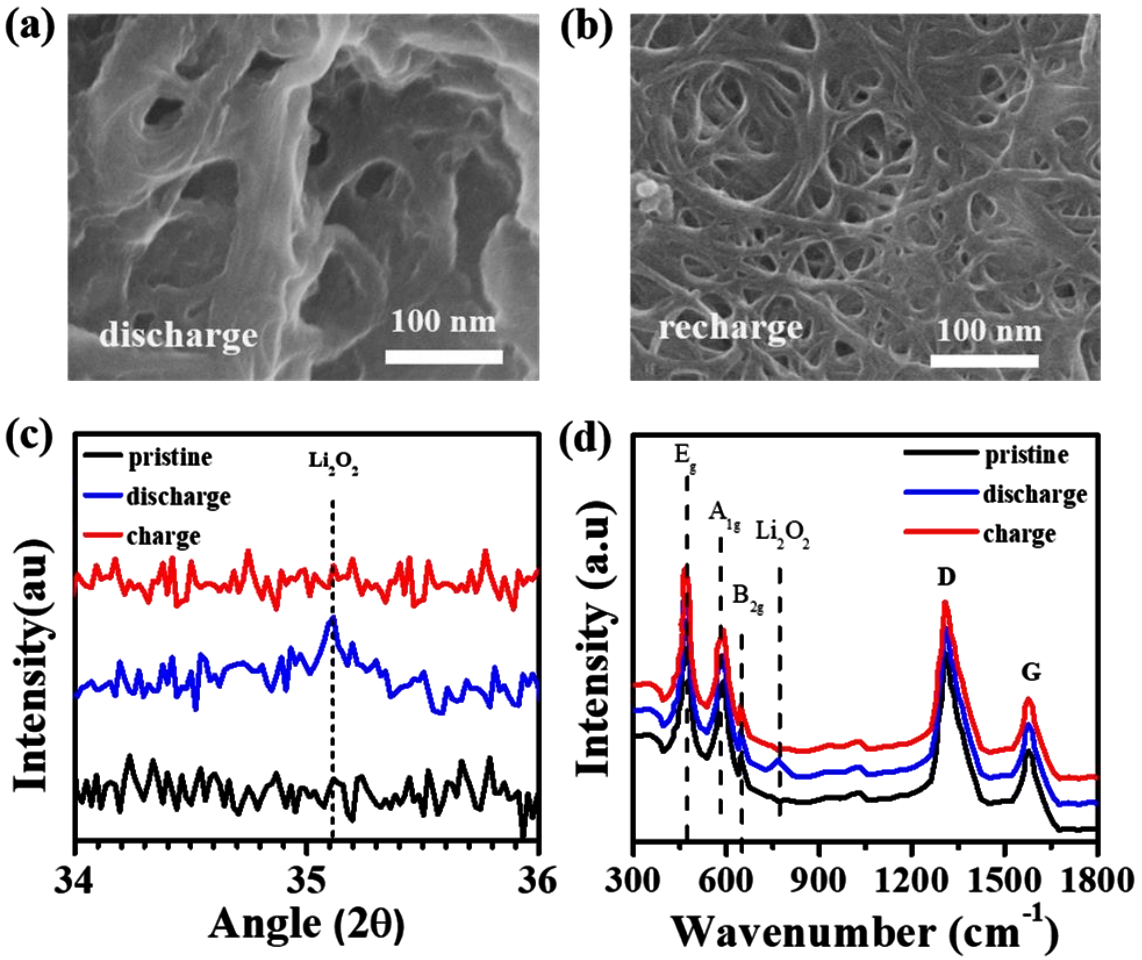

Figure 5. SEM images of (a) fully discharged and (b) recharged cathode of CNT/RuO_2 (c) XRD and (d) Raman spectrum of pristine, discharged, and recharged cathode of CNT/RuO_2 in polymer based Li-O_2 batteries.

Further investigations were obtained conducting XRD test to study the creation and breakdown of Li_2O_2 during discharge and charge process as demonstrated in Fig. 5c. A clear peak of Li_2O_2 can be observed in the discharge cathode, which indicates that the leading product was Li_2O_2 during the discharge process of Li-O_2 battery with CNT/RuO_2 cathode and polymer electrolyte [48]. Moreover, in recharge process the diffraction peak for Li_2O_2 disappear, which clearly shows that discharge and charge is associated with reversible accumulation and disintegration of Li_2O_2. For further confirmation, Raman technique has been used to gain additional information about the deposition of RuO_2 on carbon nanotubes as shown in the Fig. 5(d). Moreover, the fully discharge and charge cathodes were also compared with the pristine cathode to confirm the reversible formation and decomposition of discharge

product Li_2O_2. In pure CNTs and CNT/RuO_2 cathodes, the characteristic bands at around 1329 and 1574 cm^{-1} were appeared which can be allocated to D band and G band of CNTs. The band intensities for the D and G band in CNT/RuO_2 cathodes were much smaller than pristine cathode, which clearly indicate the large deposition of RuO_2 on CNT surface. In the Raman spectrum, three additional peaks were found at 509, 627, and 685 cm^{-1} in the CNT/RuO_2 cathode. Which correspond to the three Raman modes for RuO_2: E_g, A_{1g}, and B_{2g} modes, respectively. Additionally, the reversibility of Li_2O_2 accumulation and disintegration on the cathode surface is also established by ex-situ Raman spectra. After fully discharge, the typical peak for Li_2O_2 can be seen, while on the recharge cathode, it completely disappears clearly shows the reversibility of Li-O_2 battery.

4. CONCLUSION

In summary, a binder-free composite cathode of CNT/RuO_2 has been developed using a simple vacuum filtration method, in which carbon nanotubes (CNTs) defect sites were coated with RuO_2 catalyst for 400 cycles by Atomic Layer Deposition method. The surface engineering of CNTs (highly reactive for Li_2O_2) with RuO_2 catalyst avoid it from parasitic reactions. Consequently, the improved electrochemical performance in polymer-based Li-O_2 battery is attributed to the incorporation of RuO_2 catalyst in binder-free cathode. The lower potential gap of ~0.9 V has revealed the efficient role of RuO_2 catalyst for better electrochemical activities. Furthermore, the efficient electrochemical performance of Li-O_2 battery could be ascribed to the film-like morphology of discharge product. As a result, these findings could pave the way for surface modification of binder-free cathodes as a viable strategy for improving Li-O_2 battery electrochemical performance.

ACKNOWLEDGMENTS
The authors would also like to acknowledge the support from Taif University Researchers Supporting Project Number (TURSP-2020/264), Taif University, Taif, Saudi Arabia.

References

1. D. Aurbach, B. D. McCloskey, L. F. Nazar & P. G. Bruce, *Nat. Energy.*, 1 (2016) 1-11.
2. R. Black, B. Adams, L. F. Nazar, *Adv. Energy Mater*., 2 (2012) 801-815.
3. P.G. Bruce, S. A. Freunberger, L. J. Hardwick & J.M. Tarascon, *Nat. Mater.*, *11* (2012) 19-29.
4. A. C. Luntz, and B. D. McCloskey, *Chem. Rev.*, 114 (2014) 11721-11750.,
5. J. Winsberg, T. Hagemann, T. Janoschka, M.D. Hager, U. S. Schubert. *Angew. Chem. Int. Ed*, *56* (2017) 686-711.
6. W. Walker, V. Giordani, J. Uddin, V. S. Bryantsev, G. V. Chase, and D. Addison, *J. Am. Chem. Soc.*, *135* (2013) 2076-2079.
7. T. Zhang & H. Zhou. *Nat. Commun.*, 4 (2013) 1817.
8. B. D. Adams, R. Black, Z. Williams, R. Fernandes, M. Cuisinier, E.J. Berg, P. Novak, G. K. Murphy, L. F. Nazar, *Adv. Energy Mater.*, *5* (2015) 1400867.
9. Z. Liu, J. Huang, Y. Zhang, B.Tong, F.Guo, J. Wang, Y. Shi, R. Wen, Z. Zhou, L. Guo, Z. Peng, *Adv. Energy Mater.*, *9* (2019) 1901967.

10. D. U. Lee, P. Xu, Z. P. Cano, A. G. Kashkooli, M.G. Parka and Z. Chen, *J. Mater. Chem. A.*, *4* (2016) 7107-7134.
11. G. Wu, A. Santandreu, W. Kellogg, S. Gupta, O. Ogoke, H. Zhang, H-L. Wang, L. Dai. *Nano Energy.*, 29 (2016) 83-110.
12. J.J. Han, N. Li, T.Y. Zhang. *J. Power Sources.*, 193 (2009) 885-889.
13. S. Ganapathy, B. D. Adams, G. Stenou, M. S. Anastasaki, K. Goubitz, X-F. Miao, L. F. Nazar, and M. Wagemaker. *J. Am. Chem. Soc.*, 136 (2014) 16335-16344.
14. E. Nasybulin, W. Xu, M. H. Engelhard, Z. Nie, X.S. Li, J-G. Zhang. *J. Power Sources.*, 243 (2013) 899-907.
15. R. Younesi, M. Hahlin, F. Björefors, P. Johansson, and K. Edström. *Chem. Mater.*, 25 (2013) 77-84.
16. P. Lou, C. Li, Z. Cui and X. Guo. *J. Mater. Chem. A.*, 4 (2016) 241-249.
17. T. Zhang, B. Zou, X. Bi, M. Li, J. Wen, F. Huo, K. Amine, and J. Lu. *ACS Energy Lett.*, 4 (2019) 2782-2786.
18. H. Lee, D. J. Lee, M. Kim, H. Kim, Y. S. Cho, H. J. Kwon, H. C. Lee, C. R. Park, and D. Im. *ACS Appl. Mater. Interfaces*, 12 (2020) 17385-17395.
19. Q. Lin, Z. Cui, J. Sun, H. Huo, C. Chen, and X. Guo. *ACS Appl. Mater. Interfaces*, 10 (2018) 18754-18760.
20. J.H. Lee, H.W. Jung, I.S. Kim, M. Park, H.S. Kim. *Energies*, 14 (2021) 4196.
21. Y. Bae, D-H. Ko, S. Lee, H-D. Lim, Y-J. Kim, H-S. Shim, H. Park, Y. Ko, S. K. Park, H. J. Kwon, H. Kim, H-T. Kim, Y-S. Min, D. Im, K. Kang. *Adv. Energy Mater.*, 8 (2018) 1702661.
22. S. Li, M. Wang, Y. Yao, T. Zhao, L. Yang, and F. Wu. *ACS Appl. Mater. Interfaces.*, 11 (2019) 34997-35004.
23. J. Xie, X. Yao, Q. Cheng, I. P. Madden, P. Dornath, C-C. Chang, W. Fan, D. Wang. *Angew. Chem. Int. Ed.*, 127 (2015), 4373-4377.
24. Q-C. Liu, L. Li, J-J. Xu, Z-W. Chang, D. Xu, Y-B. Yin, X-Y. Yang, T. Liu, Y-S. Jiang, J-M. Yan, X-B. Zhang *Adv. Mater.*, 27 (2015) 8095-8101.
25. L. Ma, T. Yu, E. Tzoganakis, K. Amine, T. Wu, Z. Chen, J. Lu. *Adv. Energy Mater.*, *8* (2018), 1800348.
26. Y. Yang, W. Liu, N. Wu, X. Wang, T. Zhang, L. Chen, R. Zeng, Y. Wang, J. Lu, L. Fu, L. Xiao, and L. Zhuang. *ACS Appl. Mater. Interfaces*, 9 (2017) 19800-19806.
27. Y. Hou, J. Wang, J. Liu, C. Hou, Z. Xiu, Y. Fan, L. Zhao, Y. Zhai, H. Li, J. Zeng, X. Gao, S. Zhou, D. Li, Y. Li, F. Dang, K. Liang. *Adv. Energy Mater.*, 9 (2019) 1901751.
28. A. Débart, A. J. Paterson, J. Bao, P. G. Bruce. *Angew. Chem. Int. Ed.*, 47 (2008) 4521-4524.
29. K. R. Yoon, K. Shin, J. Park, S-H. Cho, C. Kim, J-W. Jung, J. Y. Cheong, H. R. Byon, H. M. Lee, and I-D Kim. *ACS Nano*, 12 (2018) 128-139.
30. J. Yi, K. Liao, C. Zhang, T. Zhang, F. Li, and H. Zhou. *ACS Appl. Mater. Interfaces.*, 7 (2015) 10823-10827.
31. Q-C. Zhu, S-M. Xu, M. M. Harris, C. Ma, Y-S. Liu, X. Wei, H-S. Xu, Y-X Zhou, Y-C Cao, K-X. Wang, J-S. Chen. *Adv. Funct. Mater.*, 26 (2016) 8514-8520.
32. Y. Wang, J. Wang, X Zhao, W. Qiu, E. Song, W. Zhang, X. Liu and J. Liu. *Energy Environ. Sci.*, 13 (2020) 2540-2548.
33. Z.Hou, S. Feng, P. Hei, T. Yang, Z. Ran, R. Zheng, X. Liao, C. Shu, J. Long. *J. Power Sources*, 441 (2019) 227168.
34. F. Li, D-M. Tang, T. Zhang, K. Liao, P. He, D. Golberg, A. Yamada, H. Zhou. *Adv. Energy Mater.*, 5 (2015) 1500294.
35. M. Song, H. Tan, X. Li, A-I. Y. Tok, P. Liang, D. Chao, H. J. Fan. *Small Methods,* 4 (2020) 1900274.
36. J. Xie, X. Yao, Q. Cheng, I. P. Madden, P. Dornath, C-C. Chang,W, Fan, D. Wang. *Angew. Chem. Int. Ed.*, 127 (2015) 1–6.
37. J-W. Jung, D-W. Choi, C. K. Lee, K. R. Yoon, S. Yu, J. Y. Cheong, C. Kim, S-H. Cho, J-S. Park, Y.

J. Park, I-D. Kim, *Nano energy.,*46 (2018) 193-202.
38. E. Yilmaz, C. Yogi, K. Yamanaka, T. Ohta, H.R. Byon, *Nano Lett*., 13 (2013) 4679-4684.
39. H-S Shin, G. W. Seo, K. Kwon, K-N. Jung, S. I. Lee, E. Choi, H. Kim, J-H. Hwang, and J-W. Lee. *APL Mater.*, *6* (2018) 047702.
40. C. Zhao, C. Yu, M. N. Banis, Q. Sun, M. Zhang, X. Li, Y. Liu, Y. Zhao, H. Huang, S. Li, X. Han, B. Xiao, Z. Song, R. Li, J. Qiu, X. Sun. *Nano Energy.*, 34 (2017) 399-407.
41. F. Li, D-M. Tang, T. Zhang, K. Liao, P. He, D. Golberg, A. Yamada, H. Zhou. *Adv. Energy Mater.*, 5 (2015) 15002941-6.
42. Z. Lin, X. Guo, H. Yu. *Nano Energy*, 41 (2017) 646-653.
43. M. Mushtaq, X.W. Guo, J.P. Bi, Z.X. Wang, H.J. Yu. *Rare Met*, 37 (2018), 520-526.
44. M. Mushtaq, X.W. Guo, Y. Wang, L. Hao, Z. Lin, and H. Yu. *ACS Appl. Mater. Interfaces*, 1 (2020) 30259-30267.
45. Z. Lyu, L. Yang, Y. Luan, X. R. Wang, L. Wang, Z. Hu, J. Lu, S. Xiao, F. Zhang, X. Wang, F. Huo, W. Huang, Z. Hu, W. Chen. *Nano energy,* 3 (2017, 68-75.
46. Y. Zhang, L. Wang, X. Zhang, L. Guo, Y. Wang, Z. Peng. *Adv. Mater*, 30 (2017) 1705571.
47. F. Sultana, K. Althubeiti, K. M. Abualnaja, J. Wang, A. Zaman, A. Ali, S. A. Arbab, S. Uddin and Q. Yang. *Dalton Trans*, 50 (2021) 16386-16394.
48. 48. K-N. Jung, J-I. Lee, J-H. Jung, K-H. Shina and J-W. Lee *Chem. Commun.*, 50 (2014) 5458-5461.
49. Z. Guo, C. Li, J. Liu, X. Su, Y. Wang and Y. Xia. *J. Mater. Chem. A.,* 3 (2015) 21123-21132.
50. C. Xiang, W. Sheng, P. Zhang, S. Zhang, J. Li, Y. Zhou, L. Huang and S. Sun. *Sci. China Mater.*, 64 (2022) 2397-2408.
51. Y. J. Lee, S. H. Park, S H. Kim, Y. Ko, K. Kang, and Y. J. Lee. *ACS Catal*., 8 (2018) 4, 2923-2934.
52. Y. Gong, X. Zhang, Z. Li, Z. Wang, C. Sun, and L. Chen. *ChemNanoMat.*, 3 (2017) 485-490.
53. P. Xu, C. Chen, J. Zhu, J. Xie, P. Zhao, M. Wang. *J. Electroanal. Chem*., 842 (2019) 98-106.
54. C. Hou, J. Han, P. Liu, G. Huang, and M. Chen. *Nano Lett*., 20 (2020) 2183-2190.
55. K. R. Yoon, G. Y. Lee, J-W. Jung, N-H. Kim, S. O. Kim, and I-D. Kim. *Nano Lett*., 16 (2016) 2076–2083.
56. H. Jang, A. Zahoor, J. S. Jeon, P. Kim, Y. S. Lee, and K. S. Nahm. *J. Electrochem. Soc.,* 162 (2015) A300-A307.
57. G. Wang, L. Huang, W. Huang, J. Xie, G. Du, S. Zhang, P. Zhu, G. Cao and X. Zhao., *Nanoscale,* 7 (2015) 20614-20624.